Journal of Alloys and Compounds 509 (2011) 7009–7015

Contents lists available at ScienceDirect

Journal of Alloys and Compounds

journal homepage: www.elsevier.com/locate/jallcom

Hydrothermal synthesis and characterization of mesoporous zinc selenide agglomerates by nitrogen bubble templates

Hung-Yin Lin[a], Jyh-Ding Wei[b], Chia-Chih Ou[a], Jin-Wei Lu[c], Chen-Yi Tsai[c], Mei-Hwa Lee[c,*]

[a] Department of Chemical and Materials Engineering, National University of Kaohsiung, Kaohsiung 81148, Taiwan
[b] The Minimal Invasive Surgery Department of Orthopedics, West Garden Hospital, Taipei, Taiwan
[c] Department of Materials Science and Engineering, I-Shou University, Kaohsiung 84001, Taiwan

ARTICLE INFO

Article history:
Received 9 February 2011
Received in revised form 22 March 2011
Accepted 1 April 2011
Available online 16 April 2011

Keywords:
Hydrothermal synthesis
Zinc selenide
Mesoporous material
Nanoparticles

ABSTRACT

Mesoporous coral-like and litchi-like zinc selenide agglomerates were successfully synthesized with sodium selenite and zinc acetate dihydrate as precursors by adding hydrazine hydrate using the hydrothermal method. The experimental parameters were varied and hard agglomerates of small nanoparticles were observed. Increasing amounts of hydrazine hydrate were added to control the pH values of the reaction system. The effective control of the morphology and size of the ZnSe nanopores agglomerates by varying the pH was also demonstrated. The N_2 bubble templates produced provided the aggregation centers during the reaction, and then result in agglomerates of the small ZnSe nanoparticles with mesopores. The litchi-like zinc selenide has two different morphologies, including hollow spherical agglomerates comprising of 4–8 nm diameter nanoparticles and 15–25 nm diameter nanorods. The coral-like ZnSe mesoporous structure has a very high specific surface area of 129 m^2/g and an emission band at 626 nm as measured by a photoluminescence (PL).

1. Introduction

According to the definition of pore size by the International Union of Pure and Applied Chemistry (IUPAC), porous materials are divided into three classes – *macropores* with pore sizes of over 50 nm; *mesopores* with pore sizes from 2 nm to 50 nm, and *micropores* with pore sizes under 2 nm [1]. Mesoporous materials have been used in catalysis, gas sensors, separation, drug delivery, tissue engineering and other applications. Owing to their extremely high surface area to mass ratios, even small quantities of such materials can support various processes with high efficiency [2].

Zinc selenide (ZnSe) as a wide direct band gap (2.67 eV) II–VI semiconductor material has been regarded as a potential material for optoelectronic devices, such as blue laser diodes, light emitting diodes, solar cells and photo detectors [3,4]. Because of its low absorptivity at infrared wavelengths, its visible transmission and very high photosensitivity, ZnSe is a promising material for use in windows, lenses, output couplers, beam expanders, and optically controlled switches [5]. The morphology of ZnSe materials has been controlled using a variety of wet chemical syntheses, such as the sonochemical method [6], surfactant-assisted chemistry methods [7], reverse micelle synthesis [8], the solvothermal method [9–11], and sol–gel methods [12,13]. Recently, numerous investigations have successfully demonstrated the synthesis of zinc selenide with various geometrical morphologies, including those of nanoparticles [10,14], wires [15,16], belts [17], rods [18,19], needles [20], saws and tubes [21,22], hollow microspheres [9,23], plates [24,25] and flowerlike [20,26] patterns of radially aligned nanoflakes [27].

Previous studies have shown that the bubbles created by adding gas producing chemicals could be used as templates. During the reaction, nuclei particles may precipitate and aggregate around the gas–liquid interface to form the hollow structures [9,28,29]. Applications of porous semiconductors whose properties differ completely from those of the bulk material include various novel sensors, electrodes for use in fuel cells and others [30,31]. Since water is an environmentally friendly reaction medium, the hydrothermal method is a green process and ready for commercial adoption. The reactions are performed in a closed system and the contents are easily recovered and reused after cooling to room temperature [32,33]. Numerous compounds have been utilized to prepare powders using a hydrothermal method. Notably, hydrothermally obtained powders with different microstructures, morphologies and phase compositions are generated by varying different parameters, such as temperature, pressure and the reaction time [32,33].

In this study, mesoporous ZnSe agglomerates were prepared using the hydrothermal method from sodium selenite and zinc acetate dihydrate as precursors by adding aqueous hydrazine

* Corresponding author at: Department of Materials Science and Engineering, I-Shou University, No. 1, Sec. 1, Syuecheng Rd., Dashu District, Kaohsiung City 84001, Taiwan. Tel.: +886 7 657 7711x3128; fax: +886 7 657 8444.
E-mail address: meihwalee@ntu.edu.tw (M.-H. Lee).

0925-8388/$ – see front matter © 2011 Elsevier B.V. All rights reserved.
doi:10.1016/j.jallcom.2011.04.022

hydrate. N_2 bubble templates were produced to provide the aggregation centers during the reaction, and then result in agglomerates of the small ZnSe nanoparticles at different pH values. Furthermore, the mechanism of the ZnSe agglomerates formation at various pH values was examined. The structural characterization and the N_2 adsorption–desorption isothermal property of these ZnSe agglomerates were examined with the addition of hydrazine hydrate, which was used to control the pH of the reaction system. In addition, the optical properties of ZnSe agglomerates were investigated. This work represents the first case of litchi-like and coral-like mesoporous ZnSe structures reported in the literature.

2. Experimental procedure

2.1. Synthesis

Zinc acetate dihydrate (0.01 mol), sodium selenite (0.01 mol) and 30 ml deionized water were placed in a 250 ml beaker. The mixture was stirred using a magnetic stirrer for 15 min at room temperature to produce a milky solution. This solution was then transferred to a Teflon-lined stainless steel autoclave and aqueous hydrazine hydrate was added in an amount that was easily adjusted from 10 to 50 ml to synthesize various ZnSe morphologies. The mixture was stirred using a magnetic stirrer bar and then deionized water was added up to a maximum volume of 70% of the total. The pH was then immediately measured using a pH meter. All of the reactants were analytical grade and used without further purification.

The autoclave was sealed and heated to 180–230 °C. It was maintained for 2 h and then allowed to cool without intervention to room temperature. The resulting orange yellow precipitate was collected from the bottom of the autoclave. The powder was filtered and washed three times using distilled water and ethanol until the color changed from light orange yellow to dark yellow. Finally, the zinc selenide (ZnSe) powder was dried overnight in a dryer (~30 °C).

2.2. Characterization of ZnSe agglomerates

The microstructure of the zinc selenide (ZnSe) sample was characterized with a Hitachi S-4700 field emission-scanning electron microscope (FE-SEM; Tokyo, Japan). An energy-dispersive X-ray spectrometer was used to perform a chemical microanalysis in conjunction with a field emission-scanning electron microscope (FE-SEM) to determine the elemental constitution of ZnSe. The X-ray diffraction analysis (D8 Advance XRD, Bruker, Germany) was used to determine the crystalline structure of the ZnSe powder. The high resolution transmission electron micrographs (HRTEM) of ZnSe samples were obtained by using Tecnai G^2 20 S-Twin instrument (FEI Company, Hillsboro, OR, U.S.A.), operating at 200 kV. The N_2 adsorption–desorption isotherms were measured at 77 K using a NOVA® Surface Area Analyzer (NOVA 1000, Quantachrom, U.S.A.). The specific surface area and pore size distribution of the ZnSe powder were obtained using the multipoint Brunauer–Emmett–Teller (BET) method. The pore-size distribution was thus calculated using the Barrett–Joyner–Halenda (BJH) method. The ZnSe particles were monitored with a fluorescence spectrophotometer (F-7000, Hitachi Co., Japan) with excitation wavelengths from 200 to 500 nm.

3. Results and discussion

3.1. Effect of synthesis temperature on the particle size

The effect of the reaction temperature on the size of ZnSe particles was examined. Fig. 1 presents the effect of the reaction temperature from 180 °C to 230 °C on the mean size of ZnSe agglomerates. The inset in Fig. 1 displays SEM images of ZnSe agglomerates that had been prepared at 180 °C and 190 °C. The mean size of ZnSe agglomerates at 180 °C (152 nm) was much smaller than at 190 °C (457 nm). The size of agglomerates of ZnSe changed dramatically with the reaction temperature from 180 °C to 190 °C. As the reaction temperature increased from 190 °C to 230 °C, the mean size of the agglomerates was increased slightly to approximately 510 nm. The mean size of ZnSe agglomerates increased with increasing reaction temperature because the high temperature heat treatment resulted in particle growth and agglomeration. The results show that the reaction temperature played an important role in agglomeration behavior of the ZnSe nanoparticles.

Fig. 2 shows X-ray diffraction (XRD) patterns of ZnSe agglomerates synthesized at (a) 180 °C, (b) 190 °C, (c) 200 °C, (d) 210 °C and (e) 220 °C, respectively. The diffraction peaks in the samples

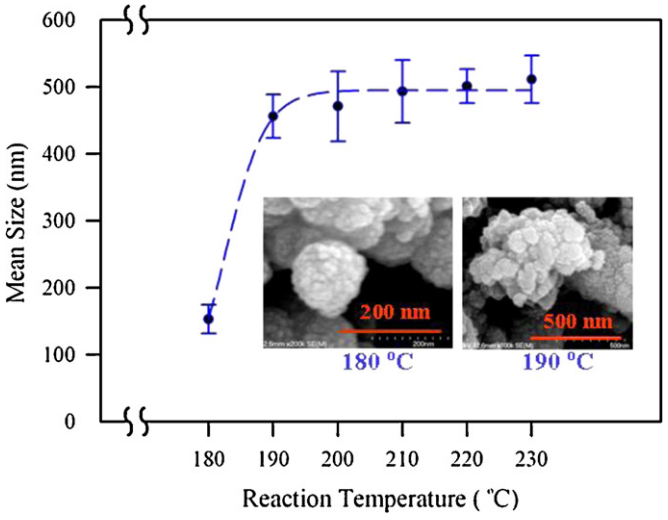

Fig. 1. Mean size of ZnSe powder at various reaction temperatures. Inset: SEM images of the synthesized ZnSe powder at 180 °C and 190 °C.

corresponded to (111), (200), (220), (311), (400), and (331) indicating that the ZnSe powder was cubic zinc blende structure (JCPDS card #05-0522) in Fig. 2(a)–(d). Fig. 2(a)–(e) showed that crystallinity improved with increasing of reaction temperature. The XRD patterns of the ZnSe agglomerates prepared at the three temperatures in the range of 200–220 °C were essentially identical, but those at 180 °C and 190 °C were not. As shown in Fig. 2(a) and (b), three extra unidentified peaks (labeled with *) were observed for samples prepared at 180 °C and 190 °C. This is an indication that the ZnSe agglomerates at 180 °C and 190 °C were of lower purity. Furthermore, peak broadening decreased with an increase of temperature from 180 to 200 °C as shown in Fig. 2(a)–(c). This indicates that the crystallinity of ZnSe was greatly improved above 200 °C. To obtain better purity of ZnSe products with cubic zinc blende structures, 200 °C was chosen as the reaction temperature in subsequent experimental work.

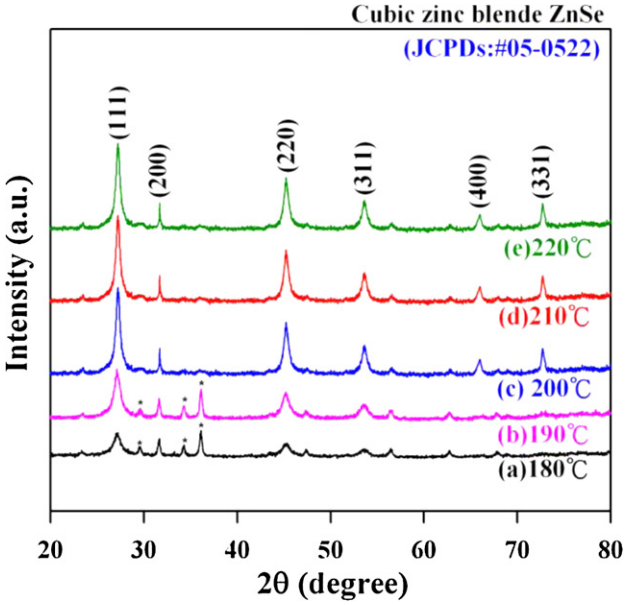

Fig. 2. X-ray diffraction pattern of ZnSe powder at reaction temperatures (a) 180 °C, (b) 190 °C, (c) 200 °C, (d) 210 °C and (e) 220 °C for 2 h.

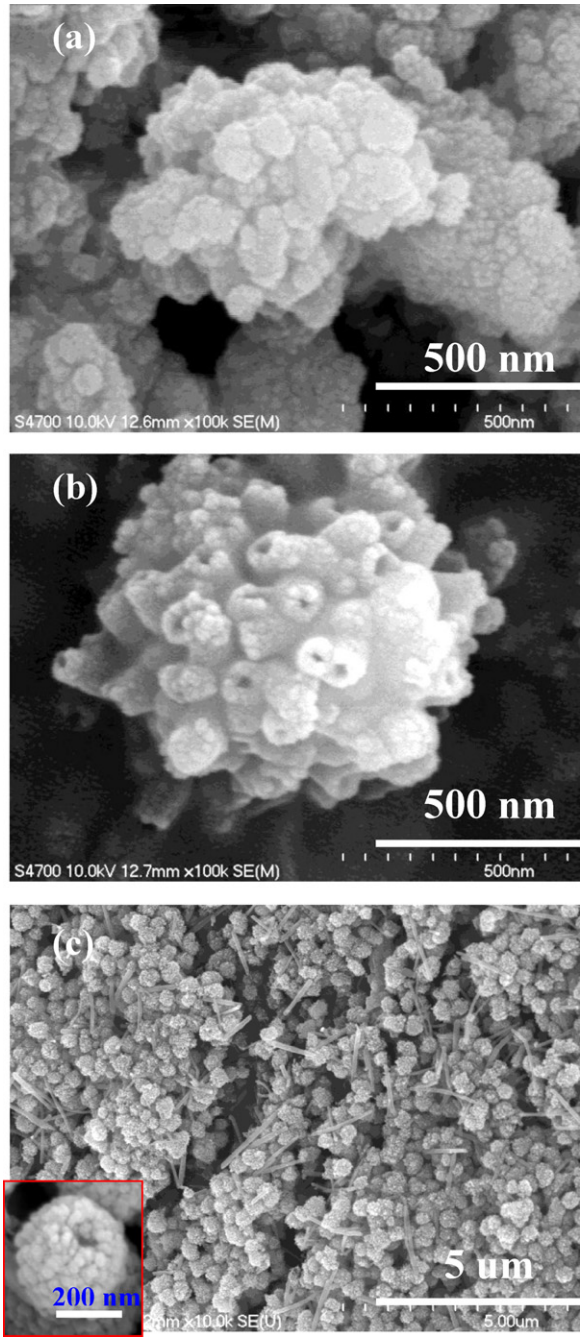

Fig. 3. SEM images of ZnSe powder synthesized at various pH values: (a) pH 9.5, (b) pH 10.5 and (c) pH 11.5 (note scale difference of images (a) and (b)).

3.2. *Effect of pH on particle size and morphologies*

ZnSe agglomerates were prepared by the hydrothermal method using a mixture of $Zn(C_2H_3O_2)_2$ and $NaSeO_3$ as the precursor, with the addition of hydrazine hydrate at 200 °C. We investigated the effect of the amount of hydrazine hydrate, which altered the pH of the reaction, on the formation of ZnSe powder. The experimental parameters were varied and hard agglomerates of small nanoparticles were observed. Fig. 3 presents FESEM images of the ZnSe agglomerates obtained at various pH values: (a) pH 9.5, (b) pH 10.5 and (c) pH 11.5. Irregular, coral-like and litchi (Chinese fruit)-like patterns of ZnSe agglomerates, as shown in Fig. 3(a)–(c), were obtained at pH values of 9.5, 10.5 and 11.5, respectively. ZnSe agglomerates formed hard agglomerations at all three pH values. However, at pH 9.5, the agglomerates were 700 nm in size and composed of ZnSe nanoparticles, but were irregular and had no pores (Fig. 3(a)). Mesopores, 20–50 nm, were observed in the agglomerates at pH 10.5 and 11.5 as shown in Fig. 3(b) and (c). At pH 10.5, the morphologies of the obtained ZnSe agglomerates were coral-like, and each contained many 20–50 nm pores as shown in Fig. 3(b). The ZnSe litchi-like patterns, observed at pH 11.5, included hollow spherical agglomerates of 300 nm with nanorods of 2–4 μm. Each hollow spherical agglomerate contained one ~50 nm pore. The morphologies of agglomerates of ZnSe nanoparticles depended markedly on the pH values in the reactor (and therefore on the amount of hydrazine hydrate added). Crystallization kinetics (primary nucleation, crystal growth, and agglomeration) of ZnSe depended on supersaturation, stirrer speed, pH, molar feed ratio and residence time [34]. It is very difficult to estimate the relationship between agglomeration and crystal growth kinetics [35]. However, the SEM images showed that for the obtained agglomerates, pH significantly affected the formation of the mesoporous structure at high pH. The formation of ZnSe can be formulated by Eq. (1) as follows:

$$2SeO_3^{2-} + 2ZnO_2^{2-} + 3N_2H_4 \rightarrow 2ZnSe \downarrow + 3N_2 \uparrow + 2H_2O + 8OH^- \quad (1)$$

Liu et al. reported that the reduction of power by N_2H_4 is directly related to the pH value of the reaction system [36]. N_2 bubbles which were produced in the reaction were used as templates to synthesize ZnSe [37,38] or CdSe [36] hollow microspheres. Scheme 1 shows that the possible mechanism of ZnSe agglomeration depends on the pH. According to the nucleation theory [39], there are a larger number of ZnSe nuclei at higher pH values due to supersaturation. Furthermore, ZnSe nuclei and N_2 bubble nuclei gradually grow into ZnSe nanoparticles and N_2 gas bubbles, respectively. Owing to the lower formation rate of N_2 bubbles at lower pH, such as 9.5, there are not enough N_2 bubbles to serve as aggregation centers. Therefore, ZnSe nanoparticles did not deposit on the surfaces of N_2 bubbles but aggregate with each other to form irregular morphology with no porosity, as shown in the route 1. Moreover, the moving speed of N_2 bubbles was not fast enough to induce N_2 bubbles coalescence because of ZnSe nanoparticle-related flow resistance, as shown in the route 2. Nevertheless, the ZnSe nanoparticles lead to coalescence of N_2 bubbles at high pH 10.5 and ZnSe nanoparticles grow on the template of coalescence of N_2 bubbles, resulting in the formation of coral-like structures. In Scheme 1, the route 3 shows that ZnSe nanoparticles can cover the N_2 bubble, causing the formation of hollow sphere-like ZnSe agglomerates at pH of 11.5. However, the excess of ZnSe nanoparticles, growing toward a linear arrangement, forms the needle structure of ZnSe, as shown in the route 3.

Chemical analysis of the particles using FE-SEM equipped with energy dispersive X-ray spectroscopy (EDX) verified the composition of the obtained ZnSe. The results of the EDX analyses of the ZnSe particles are independent of pH from 9.5 to 11.5. Fig. 4 demonstrates that ZnSe nanocrystals are composed of Zn and Se in an approximate atom ratio of 1:1, corresponding to stoichiometric ZnSe. The Pt peak observed in the spectrum was from the SEM sample holder.

The coral-like and litchi-like powders of porous ZnSe were further characterized by TEM, and the results are shown in Fig. 5(a)–(d). Fig. 5(a) shows that TEM image of coral-like powder, having agglomeration of the nanoparticles with a diameter of 12–20 nm, which was synthesized at pH 10.5. In Fig. 5(b), it can be seen that the agglomerates from small nanoparticles ranging from 8 to 15 nm in diameter and the average diameter of nanorods is about 20 nm when the pH value of reaction mixture solution was 11.5. It was found that the single nanoparticles are bigger at pH 10.5 than at pH 11.5. Fig. 5(c) and (d) shows the corresponding HRTEM images of

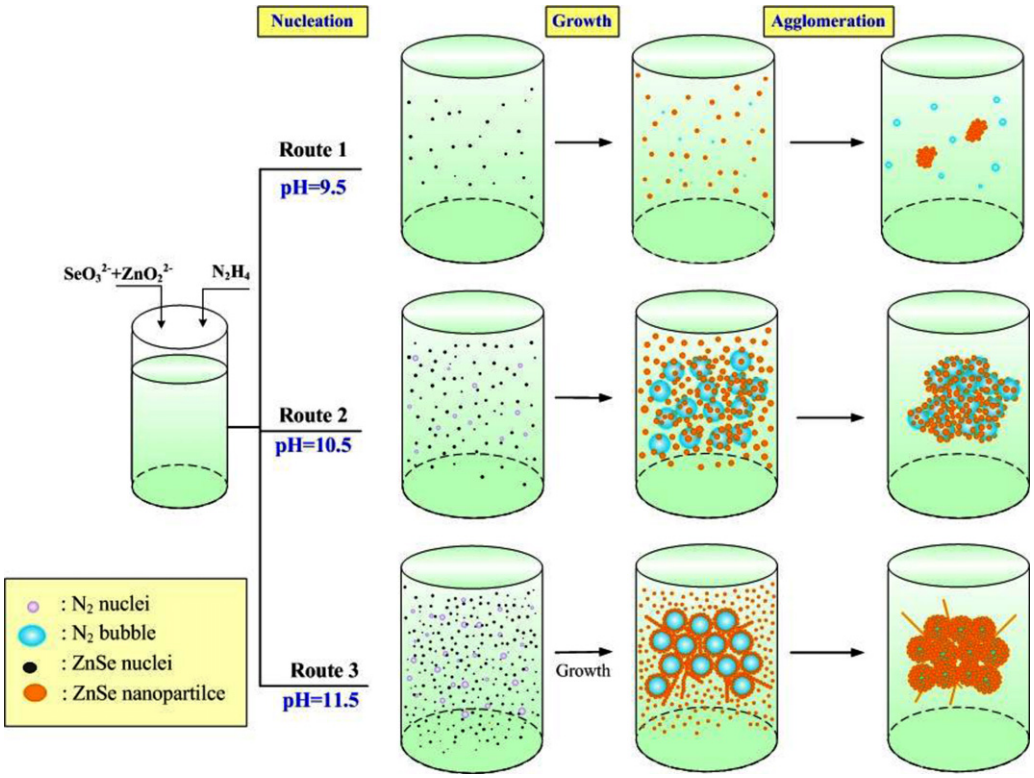

Scheme 1. Schematic illustration of the proposed mechanism of pH-dependent ZnSe agglomerate formation.

Fig. 5(a) and (b); the insets are the selected area electron diffraction (SAED) pattern having displaying six diffused rings. These diffraction rings of SAED image are assigned to be (1 1 1), (2 0 0), (2 2 0), (3 1 1), (4 0 0) and (3 3 1) of the cubic zinc blende phase of ZnSe. It reveals that the porous ZnSe samples, coral-like and litchi-like morphologies, are a polycrystalline.

3.3. The porosity properties of ZnSe samples

Fig. 6(a) presents the N_2 adsorption and desorption isotherms at 77 K for ZnSe particles at pH 9.5, 10.5 and 11.5. The pore structure of the mesoporous ZnSe agglomerate was estimated from the features of the hysteresis loop. The characteristic features of the

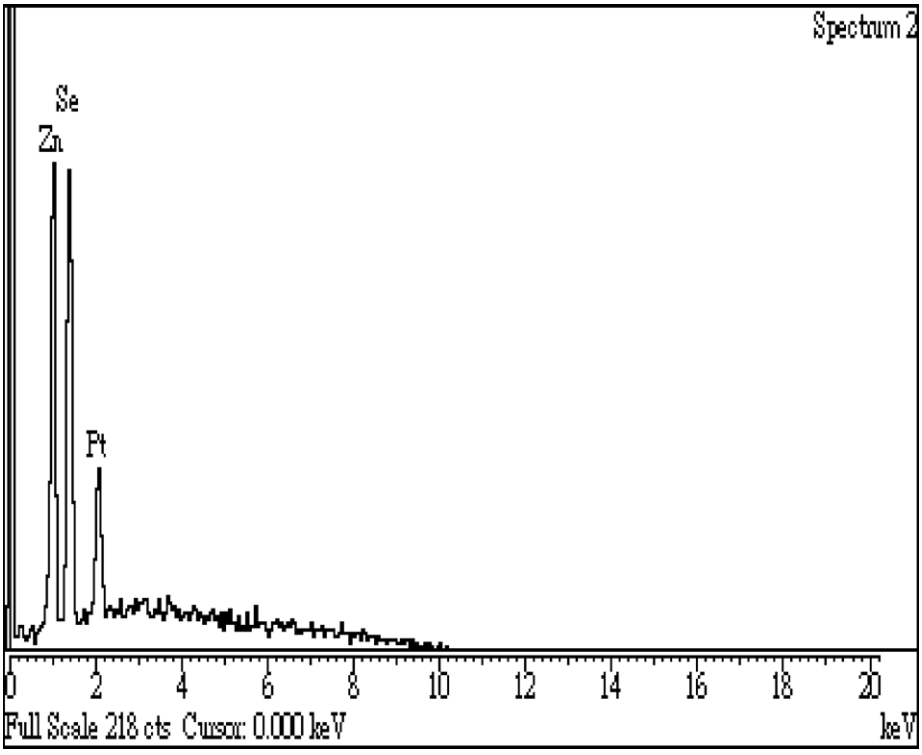

Fig. 4. EDX spectrum of ZnSe particles in Fig. 3.

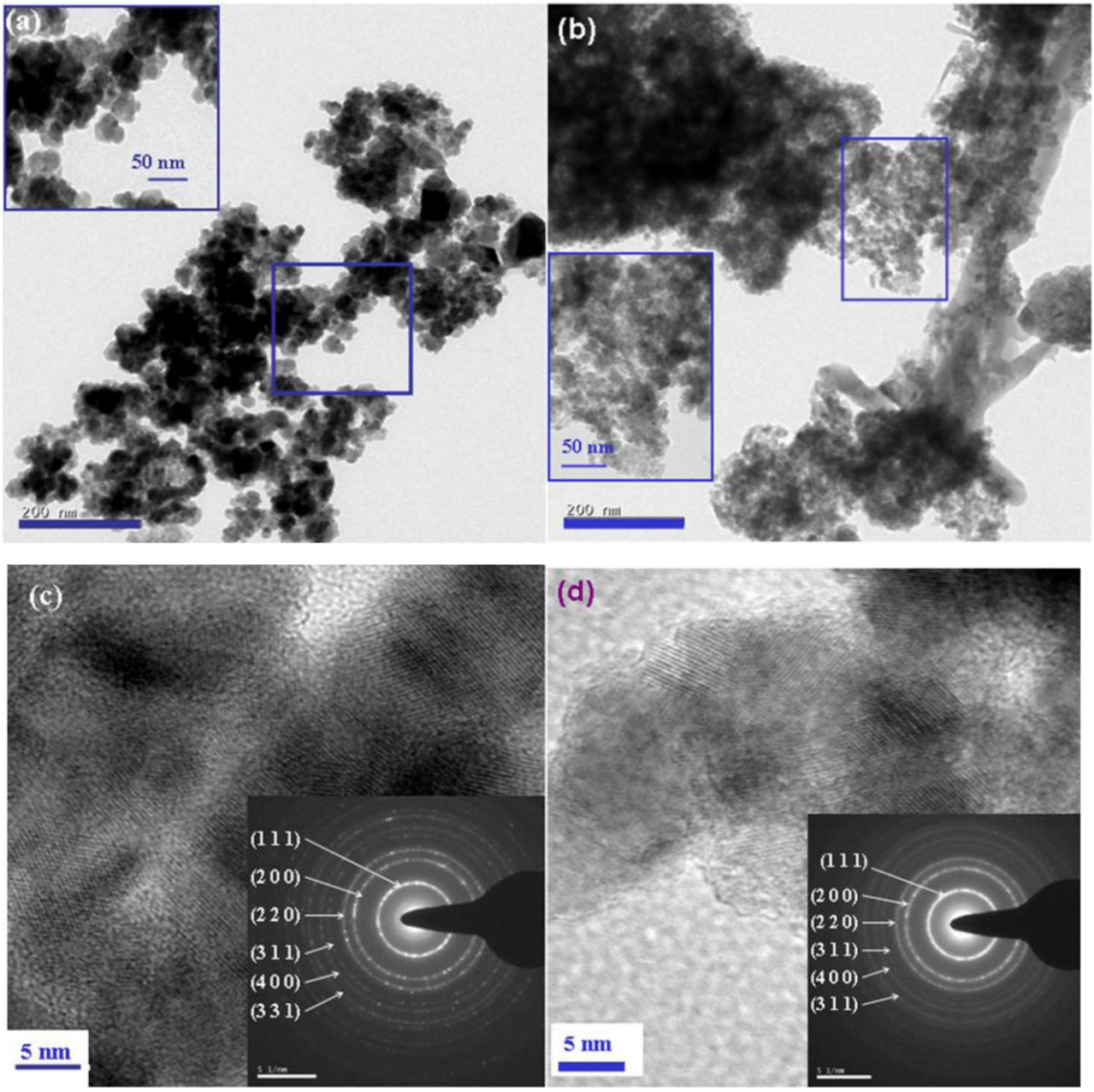

Fig. 5. TEM, SAED and HRTEM pattern images of porous ZnSe agglomerates prepared at pH 10.5 and pH 11.5. (a) and (b)TEM images of ZnSe coral-like powder (pH 10.5) and ZnSe litchi-like powder (pH 11.5), (c) and (d) HTEM images of (a) and (b), with insets is corresponding to the SAED pattern.

hysteresis loop are associated with capillary condensation in mesopores. Based on the IUPAC classification [1], a type II adsorption isotherm with no hysteresis loop was obtained at pH 9.5, revealing that ZnSe agglomerates with non-porous or macroporous adsorbents correspond to the SEM image in Fig. 3(a). The isothermal characteristics at pH 10.5 and pH 11.5 are typical of type IV. The hysteresis loops obtained at both pH 10.5 and pH 11.5 resembled the type H3 loop, which is characteristic of the mesoporous materials that contained pores of highly uniform sizes, indicating that the solid is mesoporous with cylindrical geometry of a uniform pore size and non-intersecting mesopores [40,41]. The results correspond to the SEM images in Fig. 3(b) and (c) of porous materials with pore diameters from 20 to 50 nm.

The multi-point Brunauer–Emmett–Teller (BET) method was employed to calculate the specific surface area. The specific surface area was 20.74 m^2/g at pH 9.5, 129.5 m^2/g at pH 10.5 and 42.8 m^2/g at pH 11.5, respectively. As presented in Fig. 3, at pH 10.5, the ZnSe particles had a coral-like morphology and contained numerous mesopores; at pH 11.5, they had a litchi-like morphology and contained hollow pores; at pH 9.5, they had an irregular morphology and were non-porous. Evidently, controlling the morphology of ZnSe particles is important, and the numbers of pores varies with the pH value. Fig. 6(b) showed the pore size distribution at pH 10.5 and pH 11.5. The pore sizes were calculated from the adsorption branch of the N_2 isotherm using the BJH method. The calculations showed both pore size distributions range from 2 nm to 50 nm, corresponding to the definition of mesoporous materials.

3.4. The photoluminescence spectrum of ZnSe powders

As shown in Fig. 7, the broad emission peaks were 616 nm, 621 nm and 626 nm, respectively, under the excitation at 320 nm on

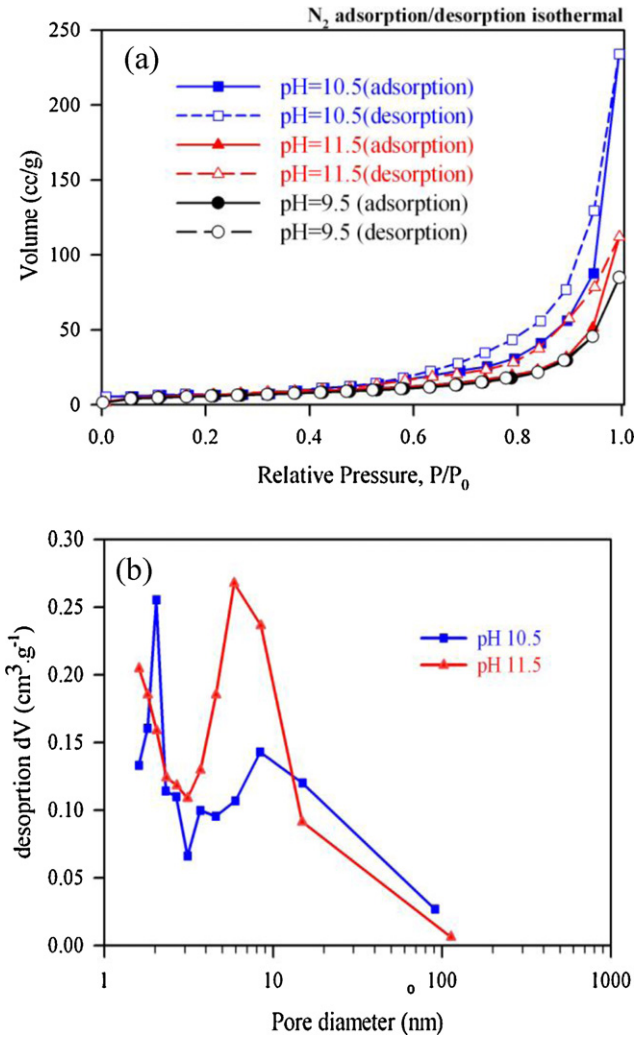

Fig. 6. (a) Nitrogen adsorption/desorption isotherms at 77 K for ZnSe agglomerates synthesized at different pH values. pH 9.5 (circle), 10.5 (triangle) and 11.5 (square) [empty symbols – desorption; filled symbols – adsorption]. (b) Corresponding pore-size distributions of ZnSe agglomerates synthesized at pH 9.5 (circle), 10.5 (triangle) and 11.5 (square) obtained by BJH method.

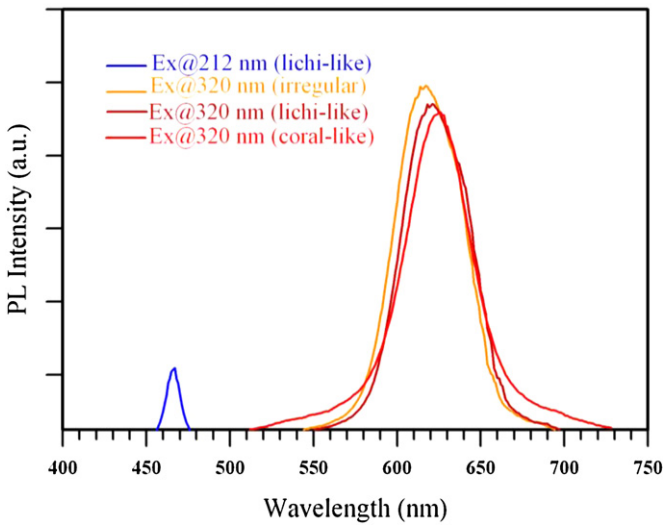

Fig. 7. Photoluminescence spectrum of the ZnSe agglomerates, synthesized at different pH, under excitation wavelengths of 212 nm and 320 nm.

irregular, litchi-like and coral-like agglomerations. Wang et al. [38] have previously reported that the PL broad peak is an indication of the small nanoparticles in spherical walls of ZnSe hollow microspheres. The weak emission peak centered at 467 nm is attributed to the near-band edge (NBE) emission of ZnSe under the excitation at 212 nm on litchi-like ZnSe agglomerates. The band gap energy of the bulk ZnSe crystal E_g was 2.67 eV (466 nm) [42]. The photoluminescence (PL) spectrum, having a weak emission at around 450 nm and a strong emission at around 620 nm, was observed in ZnSe bulk [15]. These results suggest that the morphology and pore types of ZnSe agglomerates are important factors for the emission peaks in the photoluminescence spectrum.

4. Conclusions

Mesoporous ZnSe agglomerates were prepared by the hydrothermal process at a reaction temperature of 200 °C. The mean diameter of ZnSe agglomerates increases with increased reaction temperature. Hydrazine hydrate was added to control agglomerate formation and increase the pH of the reaction system. The morphology and size of the nanopores of ZnSe agglomerates were controlled by varying the pH. Irregular, coral-like and litchi-like patterns of ZnSe agglomerates were obtained at pH values at 9.5, 10.5 and 11.5, respectively. The results show the influence of formation rate and moving speed of N_2 bubbles on the morphology of the ZnSe agglomerates. The mesopores, sized from 20 nm to 50 nm, were observed in both coral-like and litchi-like morphologies, and their cubic zinc blende phase was identified by XRD. Moreover, the mesoporous ZnSe agglomerates having high specific surface area may have the potential applications in catalysis, gas sensors, separation and drug delivery.

Acknowledgements

The authors would like to thank the National Science Council of the Republic of China, Taiwan, for financially supporting this research under Contract No. NSC 96-2815-C-214 -002 -E and NSC97-2221-E-214-015.

References

[1] K.S.W. Sing, D.H. Everett, R.A.W. Haul, L. Moscou, R.A. Pierotti, J. Rouquerol, T. Siemieniewska, Pure Appl. Chem. 57 (1985) 603–619.
[2] X.S. Zhao, J. Mater. Chem. 16 (2006) 623–625.
[3] C.R. Wang, J. Wang, Q. Li, G.-C. Yi, Adv. Funct. Mater. 15 (2005) 1471–1477.
[4] S. Xiong, J. Shen, Q. Xie, Y. Gao, Q. Tang, Y. Qian, Adv. Funct. Mater. 15 (2005) 1787–1792.
[5] M.J. Tafreshi, K. Balakrishnan, R. Dhanasekaran, J. Mater. Sci. 32 (1997) 3517–3521.
[6] J. Zhu, Y. Koltypin, A. Gedanken, Chem. Commun. 12 (2000) 73–78.
[7] B. Ludolph, M.A. Malik, Chem. Commun. (1998) 1849–1850.
[8] F.T. Quinlan, J. Kuther, W. Tremel, W. Knoll, S. Risbud, P. Stroeve, Langmuir 16 (2000) 4049–4051.
[9] Q. Peng, Y. Dong, Y. Li, Angew. Chem. Int. Ed. 42 (2003) 3027–3030.
[10] W. Wang, Y. Geng, P. Yan, F. Liu, Y. Xie, Y. Qian, J. Am. Chem. Soc. 121 (1999) 4062–4063.
[11] J. Yang, G. Wang, H. Liu, J. Park, X. Gou, X. Cheng, J. Cryst. Growth 310 (2008) 3645–3648.
[12] H. Jiang, X. Yao, J. Che, M. Wang, F. Kong, Ceram. Int. 30 (2004) 1685–1689.
[13] Y. Wang, X. Yao, M. Wang, F. Kong, J. He, J. Cryst. Growth 268 (2004) 580–584.
[14] Y. Li, G.C.L. Wong, C.R. Safinya, E. Caine, E.L. Hu, D. Haeffner, P. Fernandez, W. Yun, Rev. Sci. Instrum. 69 (1998) 2844–2848.
[15] Y.-C. Zhu, Y. Bando, Chem. Phys. Lett. 377 (2003) 367–370.
[16] X.T. Zhang, Z. Liu, Y.P. Leung, Q. Li, S.K. Hark, Appl. Phys. Lett. 83 (2003) 5533–5534.
[17] T. Zhai, H. Zhong, Z. Gu, A. Peng, H. Fu, Y. Ma, Y. Li, J. Yao, J. Phys. Chem. C 111 (2007) 2980–2986.
[18] A.B. Panda, G. Glaspell, M.S. El-Shall, J. Am. Chem. Soc. 128 (2006) 2790–2791.
[19] J. Yang, C. Xue, S.-H. Yu, J.-H. Zeng, Y.-T. Qian, Angew. Chem. Int. Ed. 114 (2002) 4891–4894.
[20] H. Fu, H. Li, W. Jie, L. Yang, J. Cryst. Growth 289 (2006) 440–444.
[21] J.Q. Hu, Y.S. Bando, J.H. Zhan, Z.W. Liu, D. Golberg, S.P. Ringer, Adv. Mater. 17 (2005) 975–979.

[22] A. Colli, S. Hofmann, A.C. Ferrari, C. Ducati, F. Martelli, S. Rubini, S. Cabrini, A. Franciosi, Appl. Phys. Lett. 86 (2005) 103–104.
[23] L. Zhang, H. Yang, X. Xie, F. Zhang, L. Li, J. Alloys Compd. 473 (2009) 65–70.
[24] M. Chen, L. Gao, Mater. Chem. Phys. 91 (2005) 437–441.
[25] Z.-X. Deng, C. Wang, X.-M. Sun, Y.-D. Li, Inorg. Chem. 41 (2002) 869–873.
[26] Y. Yang, F. Du, C. Miao, Mater. Lett. 62 (2008) 1333–1335.
[27] J. Du, L. Xu, G. Zou, L. Chai, Y. Qian, Mater. Chem. Phys. 103 (2007) 441–445.
[28] C. Yan, D. Xue, J. Alloys Compd. 431 (2007) 241–245.
[29] F. Gu, C.Z. Li, S.F. Wang, M.K. Lü, Langmuir 22 (2006) 1329–1332.
[30] M. Nirmal, B.O. Dabbousi, M.G. Bawendi, J.J. Macklin, J.K. Trautman, T.D. Harris, L.E. Brus, Nature 383 (1996) 802–804.
[31] H. Föll, J. Carstensen, S. Frey, J. Nanomater. 2006 (2006) 1–10.
[32] G. Demazeau, J. Mater. Chem. 9 (1999) 15–18.
[33] K. Byrappa, M. Yoshimura, Handbook of Hydrothermal Technology, second ed., William Andrew Publishing, NY, USA, 2001.
[34] M. Al-Tarazi, A.B.M. Heesink, M.O.J. Azzam, S.A. Yahya, G.F. Versteeg, Cryst. Res. Technol. 39 (2004) 675–685.
[35] H. Hatakka, P. Oinas, J. Reunanen, S. Palosaari, Acta Polytech. Scand. 244 (1997) 76–78.
[36] X. Liu, J. Ma, P. Peng, W. Zheng, Mater. Sci. Eng. B 150 (2008) 89–94.
[37] H. Wang, F. Du, Cryst. Res. Technol. 41 (2006) 323–327.
[38] X. Wang, X. Chen, H. Zheng, J. Jin, Z. Zhang, Appl. Phys. A 80 (2005) 511–513.
[39] R. Boistelle, J.P. Astier, J. Cryst. Growth 90 (1988) 14–30.
[40] J.C. Groen, L.A.A. Peffer, J. Pérez-Ramírez, Micropor. Mesopor. Mater. 60 (2003) 1–17.
[41] L. Téllez, J. Rubio, M.A. Valenzuela, F. Rubio, J.L. Oteo, Adv. Technol. Mater. Mater. Process. J. 8 (2006) 226–231.
[42] Z. Zhu, G.D. Brownlie, P.J. Thompson, K.A. Prior, B.C. Cavenett, Appl. Phys. Lett. 67 (1995) 3762–3764.